A many-to-one sensory circuit encodes oxygen levels and drives respiratory behaviour in *Danio rerio*

Chen-Min Yeh[1#], Gerald M. Pao[2,3,#], Reginno Villa-Real[1], Kaila Rosales[1], Elizabeth DePasquale[1], Alex Groisman[4] and Sreekanth H. Chalasani[1*].

[1] Molecular Neurobiology Laboratory, The Salk Institute for Biological Studies, La Jolla, CA 92037.

[2] Molecular and Cellular Biology-4, The Salk Institute for Biological Studies, La Jolla, CA 92037.

[3]Climate Atmospheric Sciences and Physical Oceanography, Scripps Institution of Oceanography, University of California San Diego, La Jolla, CA 92093.

[4] Department of Physics, University of California San Diego, La Jolla, CA 92093.

*Author for correspondence: schalasani@salk.edu (S.H.C.).

[#] *These authors contributed equally to this project*

Abstract

In most animals, respiratory activity inversely correlates with environmental oxygen levels[1,2]. However, less is known about how the underlying neural circuitry encodes oxygen information and modifies behaviours. Here, we characterize the oxygen sensing circuit and reveal sensory coding principles in a *Danio rerio* larva, an optically accessible vertebrate that increases respiration and startle-related responses under hypoxia[3]. We observe that cranial sensory neurons receive input from multiple oxygen-sensing neuroendocrine cells, and then relay this information to hindbrain targets. Moreover, hypoxia evoked increase in cranial sensory dendrite calcium events indicates an oxygen-driven change in input dimensionality, which is also represented in their cytoplasm. Additionally, we estimate that a neural code using cytoplasmic calcium events requires most of the cranial sensory neurons, whereas one integrating input dimensionality needs only a third. Furthermore, we show that purinergic signalling at the neuroendocrine cell-sensory neuron synapses drives hypoxia-induced respiratory changes, independent of serotonin, which triggers startle-related responses. Collectively we demonstrate that oxygen coding employs a "many-to-one" sensory circuit that transforms ambient oxygen into neuronal activity and input dimensionality changes to impact behaviour. More broadly, we suggest that multi-dimensional coding might be a common feature of many-to-one circuit motifs, revealing a function for related circuits across species.

Mammals have evolved specialized neural circuitry to detect and respond to oxygen changes. Neuroendocrine glomus cells in the carotid body sense blood oxygen levels and communicate this information to the carotid sinus nerve, a branch of the glossopharyngeal nerve, and the brainstem[4]. Typically, hypoxia is thought to depolarize glomus cells, which in turn release ATP and acetylcholine[5] activating the carotid sinus nerve resulting in higher respiratory rates [6,7]. In parallel, hypoxia also acts via serotonin and brainstem respiratory circuits to promote arousal[8,9]. While neural circuitry and neurotransmitters driving hypoxia-induced responses have been described, how the cranial sensory neurons encode oxygen levels and initiate changes in respiratory behaviours. To gain insights into the neuronal dynamics, we probed these pathways in the transparent zebrafish larva. Teleost fish use both the glossopharyngeal and vagal cranial sensory neurons to sense hypoxia[10]. In zebrafish, these neurons innervate the gill-localized neuroendocrine cells (NECs), potential oxygen sensors and also project centrally into the hindbrain (Fig. 1a,b). The NECs share similarities with Type I glomus cells of the mammalian carotid body: both cells are neural crest derived[4,11] and depolarize their membranes using voltage-gated potassium channels upon hypoxia exposure[12,13]. Here, we show that vagal sensory neurons integrate oxygen-evoked NEC signals by increasing their activity and input dimensionality, enhancing the animal's respiratory rate upon hypoxia stimuli.

We first probed the anatomical connections between the oxygen-sensing NECs and the vagal sensory neurons by sparsely labelling individual neurons in a *PB4;UAS:Kaede* transgenic line[14]. Afferents from the labelled neurons extend into the gill arch and form enlarged processes wrapping multiple NECs (Fig. 1c-d), providing anatomical evidence for the 'many sensors-to-one neuron' connections in the oxygen sensing neural circuit (Supplementary Video S1). To address how oxygen is encoded, we used a light sheet microscope (Fig. 1e) to monitor the neural activity of these enlarged dendritic processes from individual vagal sensory neurons in a larva expressing a calcium indicator GCaMP6s in most of its neurons[15]. These enlarged dendritic processes exhibited a significantly higher frequency of calcium events under hypoxia compared to normoxia (Fig. 1f-g; Supplementary Video S2-4), indicating that these neurons received more NEC inputs under hypoxia. Vagal sensory neurons are organized into four ganglia (1st-4th), which are bilaterally symmetric and send projections to the gill arches in an antero-posterior topographic manner (Fig. 1a,b). We also used cell ablations to analyse the axonal projections from neurons within these cranial sensory ganglia in the *PB4;UAS:Kaede* transgenics. Ablating a single neuron in the 1st vagal

ganglion eliminated the most anterior projection (Supplementary Fig. 1a-c, Supplementary Video S5, S6), while ablating one in the 2nd vagal ganglion removed the middle projection, sparing the most posterior neuron with its posterior projection (Supplementary Fig. 1d-f; Supplementary Video S7). Furthermore, ablating several neurons in the 2nd ganglion eliminated a bundle of axons projecting anteriorly (Supplementary Fig. 1g-i; Supplementary Video S8, S9). These data suggest that the anterior-posterior organization of axonal projections from the cranial ganglia into the hindbrain follows that of their neuronal soma and implies that neurons in individual vagal ganglia project to specific targets in the hindbrain.

Next, we tested whether these neurons integrate dendritic signals and alter their activity upon hypoxia. We analysed calcium responses in the neurons of both the 2nd and 3rd vagal sensory ganglia in larvae expressing a neuronal nuclei-localized GCaMP6f[16] (it is technically difficult to record from the 1st and 4th ganglia). We observed recurring calcium events lasting a few seconds in neurons of both ganglia (Fig. 1h, 1i, and Supplementary Video S10, S11), a pattern that is reminiscent of burst activity reported from various respiratory neurons[17,18]. Moreover, the frequency of these events in neurons of both ganglia (Fig. 1e, 1f, Supplementary Fig. 2a, 2b), but not amplitude (Supplementary Fig. 2c-f), was increased under hypoxia exposure. The increase of neuronal calcium events in the 2nd , but not 3rd vagal sensory ganglion was oxygen dependent ($p = 0.01$; $R^2 = 0.04$, linear regression; Supplementary Fig. 2g, 2h), but the variance of these events is likely too high for individual neurons to reliably encode oxygen levels. We then hypothesized that a population of the vagal sensory neurons transform ambient oxygen into neural information. To test our hypothesis, we randomly subsampled our data and built a linear model to predict the minimal number of neurons, similar to those found in the 2nd vagal ganglion, that are needed to encode oxygen. Our analysis predicted that at least 30 neurons would be required to model oxygen concentration ($p<0.05$) (Fig. 1j). We also found that the 2nd vagal sensory ganglion comprises of 36 neurons, implying that larvae likely use most of their vagal neurons to encode ambient oxygen. Similar population-based coding schemes have been proposed for multiple neuronal circuits including mechanosensory[19], olfactory[20] and others.

To gain further insight into the vagal sensory neurons could also represent ambient oxygen levels using the number of NEC-derived input signals ("input signal dimensionality). We found that the vagal sensory neurons receive more dendritic inputs under hypoxia when compared to those under normoxia (Fig. 2a). Traditional methods that measure signal complexity include Fourier, wavelet transforms or independent component analysis are well-

suited for human engineered systems wherein signals are comprised of linear and independent components, but not ideal for complex heterogenous biological data. Instead, Simplex Projection[21] measures non-linear complexity by leveraging Takens theorem[22], which showed that essential features of dynamics of an entire system could be revealed by analysing a single variable using lags of the observed time series (Supplementary Fig. 3). These lags are used to reconstruct the intrinsic structure of the data through an embedding to generate a manifold that has the same topology ("diffeomorphism") as the original (unknown) embedding with the original (unobserved) variables. We interrogated the signal complexity of the time series by embedding additional dimensions through the incorporation of lags in the observed time series of the neuronal calcium data (Fig. 2b). To test the quality of embedding, we predicted by two fold cross-validation an out of sample, namely a portion of the time series that was withheld from the construction of the predictive manifold (Fig. 2c). Next, we estimated the optimal embedding by identifying the dimensionality that best predicts the out of sample data (Fig. 2d). Indeed, vagal sensory neurons increased their embedding dimensions under lower oxygen conditions suggesting that they received more distinct inputs under hypoxia (Fig. 2e,f). The increase of the embedding dimension in the 2nd vagal sensory ganglion is oxygen dependent ($p = 0.01$; $R^2 = 0.10$, linear regression) with greater increases of embedding dimensions under lower oxygen conditions (Supplementary Fig. 4a, 4b). Moreover, using a linear model incorporating this embedding dimensionality, we predict that 13 instead of 30 neurons are sufficient to encode oxygen levels with a 95% confidence ($p<0.05$) (Fig. 2g), suggesting that this might be a more sensitive detection measure than a conventional population code for the many-to-one sensory circuit.

To test whether vagal sensory neurons also modulate hypoxia-induced behaviours, we used a microfluidic device made of several layers of laser-cut acrylic that allowed us to monitor larval responses to hypoxia and other stressful stimuli (Fig. 3a,b; see Methods for additional information). We observed that larva increase their rate of pectoral fin beats, a respiratory-related behaviour[23] in response to hypoxia but not to a control osmotic shock (Fig. 3c-e, Supplementary Video S12, S13). The rate of the pectoral fin beat is negatively correlated with ambient oxygen (Fig. 3g; $p<0.001$, $R = -0.74$, Spearman r). In contrast, both hypoxia and osmotic shock enhance startle-related responses (Fig. 3f). Therefore, these data suggest that the increase in pectoral fin beats is specific for overcoming oxygen deprivation, while startle-related responses are associated with multiple stressors. We then asked if the pectoral fin beat increase under hypoxia is modulated by the vagal sensory neurons. Ablating neurons in the 2nd, but not 3rd vagal sensory ganglion reduced the pectoral fin beat-rate upon

hypoxia exposure (Fig. 3h). Together, these data confirm that the 2nd vagal sensory neurons drive hypoxia-induced respiratory change, providing a behavioural readout for the population-, or embedding dimension-based neural code.

We then used small molecule agonists and antagonists to gain insights into the neurotransmitter pathways relaying oxygen information from multiple NECs to vagal sensory neurons. Previous studies have shown that adenosine triphosphate induces burst activity in the petrosal sensory neurons and drives hypoxia-induced respiratory responses[7,24]. Zebrafish larvae not only express purinergic receptors in their cranial sensory neurons but also respond to ATP agonist with increased ventilation[14,25]. We asked if purinergic signalling can activate the vagal sensory neurons and drive respiration in larval zebrafish. Animals treated with a P2 purinoceptor agonist, α,β-methyleneadenosine showed an increase in pectoral fin beat rates (Fig. 4a, 4b), suggesting that purinergic signalling modifies respiratory behaviour. We also found that ablating the 2nd, but not the 3rd ganglion attenuated the agonist-induced ventilation increase, suggesting the 2nd vagal sensory ganglion is activated by purinergic signalling to control respiration (Fig. 4c). Furthermore, treating animals with this P2 purinoceptor agonist also increases the number of calcium events in the 2nd vagal sensory neurons (Fig. 4d), indicating that the agonist targets the NEC-vagal sensory neuronal synapses. Consistently, the P2 purinoceptor antagonist, PyridoxaloPhosphate-6-Axophenyl-2',4'-DiSulfonic acid (PPADS), delayed larval ventilation rate increases without affecting the startle-related response upon hypoxia (Fig. 4e, data not shown). We also tested if acetylcholine and serotonin were involved in modifying larval respiration[11,26]. While acetylcholine did not alter any hypoxia-related responses (data not shown), serotonin treatment enhanced startle-related responses without changing ventilation rate (Fig. 4f, g). Taken together, these data suggest that NECs activate the vagal sensory neurons using purinergic signalling driving hypoxia-induced respiration.

Our studies show that vagal sensory neurons encode oxygen information and modulate hypoxia-induced behaviours through specific circuits and signalling pathways. Specifically, integrating signals from NECs using a 'many-to-one' connection, the vagal sensory neurons encode oxygen levels as the changes in number of calcium events and/or embedding dimension. We propose that the NEC-mediated purinergic signalling acting on vagal sensory neurons is key to initiating hypoxia-induced respiration increases, similar to its role in initiating nociception, pain or other mechanical sensations[27,28]. Given the similarity between the zebrafish and mammalian hypoxia-evoked neural circuitry[10], we predict that

administering purinergic agonists will activate the oxygen sensing neurons and transiently increase respiration rates in mammals.

More broadly, our observations also suggest that the larval vagal sensory neurons encode oxygen levels by altering their activity or signal dimensionality, a nonlinear measure quantifying the number of distinct inputs. Our analysis indicates that the embedding dimension is a more sensitive measurement than calcium event numbers as it only requires 13 instead of 30 neurons to encode ambient oxygen. What are the real identities of these embedding dimensions? In this case, we hypothesize that they correspond to distinct NEC signals acting via a many sensors-to-one neuron circuit motif. The dimensionality increase corresponds to the increased number of inputs received by an individual sensory neuron during hypoxia, consistent with higher dendritic activity we observed under hypoxia. This measure, however, is ambiguous, as noise in the system can greatly increase dimensionality. The many-to-one topology is fairly ubiquitous in neural circuits and is described in the mammalian oxygen sensing circuits (carotid body-glossopharyngeal afferents) and other sensory systems including mechanosensory and the auditory circuits[29,30] making this coding strategy widely applicable. Although we do not know whether nervous systems widely use a dimensionality code in their sensory circuits, the informational content is undoubtedly present and at least in the zebrafish larval oxygen-sensing circuit, it provides a more sensitive coding strategy than the activity-based coding we analysed in parallel.

Methods

Calcium imaging and analysis

The imaging setup is described previously[31]. Briefly, single 5-6 days post fertilization (dpf) *elavl3*:*H2B-GCaMP6f*[16] or *elavl3*:*GCaMP6s*[15] larva with the opercula removed 1 day prior was paralyzed with a drop of 1mg/ml alpha-bungarotoxin and then embedded in the capillary with 1% low-melting agarose. We used the light-sheet microscope system to excite a single focal plane of the cranial ganglia or their processes in the gill arch and collected the resulting emission at 90ms/frame. A peristaltic pump was used to exchange the media around the larva inducing hypoxia (Fig. 1e). Oxygen levels were measured in real time and datasets where these measurements deviated more than 10% from the expected value were excluded. Custom MATLAB scripts were used to analyse the calcium data. Neurons were identified using a constrained non-negative matrix factorization framework[17] with manual validation and fluorescent signal extracted. Calcium events were identified from the detrended $\Delta F/F$ values.

Identical parameters were used across all data sets. The MATLAB scripts were included in the Supplementary material.

Immunohistochemistry

Larvae were fixed in 4% paraformaldehyde with regions of interest labeled using the following primary antibodies: goat anti-GFP (1:200; Abcam), rabbit anti-serotonin (1:200; ImmunoStar), rat anti-serotonin (1:200; NovusBio), or rabbit anti-Kaede, (1:200; MBL), which in turn were detected using secondary donkey anti-goat Alexa Fluor 488 (1:1000; Invitrogen), goat anti-rabbit Alexa Fluor 546 (1:1000; Invitrogen), or donkey anti-rat Alexa Fluor 546 (1:1000; Invitrogen). Larvae between 4-6 days post-fertilization were imaged in 70% glycerol using a Zeiss LSM800 or Olympus FM1000-MPE system. Subsequent image processing and evaluation were performed in ImageJ.

Microfluidic device

The microfluidic device is assembled out of three parts of laser-cut acrylic (PMMA; parts 2-4 in Fig. 3a) and a glass slide (part 1 in Fig. 3a). After part 2 is bonded to the glass slide a round opening in part 2 forms a 0.9 mm deep chamber where a Tricaine-anesthetized zebrafish larva is trapped inside 2.5% low-melting agarose gel. To observe larval movements, the agarose gel is removed from areas around the gills, pectoral fins and the tail using a thin needle. After parts 3 and 4 are bonded to the top of part 2, a sealed perfusion channel with two inlets and one outlet (holes in part 4) is formed directly above the trapped animal. The flow through the device is driven by a peristaltic pump connected to the outlet. The inlets are connected to reservoirs with different media and are open one at a time.

Behavioural analysis

All the behavioural data were recorded from 5-6 dpf wildtype *wik* strain or *Tg(p2rx3.2:gfp)*^{sl1} strain[14] raised under 14/10 light cycles in E2 medium. An oxygen meter (PreSens: Fibox 4, sensor: Cat. 200000241 and cell: Cat. 200001690) was attached to the outlet to measure the oxygen concentrations of the medium in real time (5-10 sec/read). The recording setup consists of an illuminating base (Tritech Research, stereo-microscope base) with a set of lens (Scheider Inc., catalogue #s 25-1070160, 25-020178, 25-011726, 25-020155, and 25-020052) and Noldus EthoVision XT10 software. Individual regions of interest were assigned to the gill, pectoral fin, body and tail (Fig. 3b) and the movements within the regions were detected by Noldus software (heartbeat detector). The percentage of the pixels that change intensity in

individual regions was quantified to identify movements. Movement of the pectoral fin was used to identify fin beats and the coordinated movements of the body parts were used to identify startle-related movements. An example code with the parameters used in the analysis was provided in the supplementary material. Hypoxia was induced by perfusing oxygen-deprived medium (E2 bubbled with nitrogen) into the microfluidic-chamber. The oxygen range for mild hypoxia was 60-80 mmHg and 10-35 mmHg for strong hypoxia. Osmotic shock was induced by perfused 100 mM or 250 mM sodium chloride solution into the microfluidic chamber. For drug treatments, Alpha, beta-methyleneadenosine 5'-triphosphate trisodium salt (TOCRIS: Cat. 3209), PPADS tetrasodium salt (TOCRIS: Cat. 0625) and serotonin hydrochloride were dissolved into 100 mM stock in Milli-Q water and further diluted into different concentrations. Each larva was trapped and its behaviour monitored with control solution before being replaced with drug-solutions.

Simplex projection

The optimal embedding dimension of each time series is identified through simplex projection (rEDM, v0.7.2: https://cran.r-project.org/web/packages/rEDM/index.html), an implementation of time delay embedding based manifold reconstruction grounded on the Takens' theorem [21]. Briefly, for each condition, an optimal consensus fraction of the time series is assigned to build the model for the entire population attempting to represent all behaviours observed in the model library (50 mmHg control: 1:850; 50 mmHg hypoxia: 1:1000; 60 mmHg control: 1:1000; 60 mmHg hypoxia: 1:1000; 90 mmHg control: 1:973; 90 mmHg hypoxia: 1:811; 105 mmHg control: 1:900; 105 mmHg hypoxia: 1:900) while the rest is reserved to evaluate the out of sample prediction performance by two-fold cross validation. Time series were explored varying the temporal delay (tau) and the embedding dimension (E). A series of embedding dimensions ranging from E = 1 to 26 and time delays tau ranging from a single time step (90ms) to 40-time steps (3.6s) were used to evaluate the predictive ability of the model. The optimal embedding dimension is chosen based on the prediction skill as seen as the observed/predicted correlation coefficient rho. For input quality control, time series with 1 calcium event detected were excluded from the analysis as it does not allow for building of a model and the embedding dimension of neurons for which with no calcium events were detected was assigned a value of 0. For the output quality control, time series with predictability lower than 0.75 or less than 10 predictions were excluded as these were insufficiently constrained to give meaningful estimates. The test period from 17 out of 77

time series were manually adjusted so that calcium events are present both in the test and prediction periods. See also Supplementary Method for a further description.

Laser ablation

Ablations were performed on *Tg(p2rx3.2:gfp)*^{sl1} larvae at 3dpf. Larvae were paralyzed with Tricaine and mounted on cover slides with lateral view on top. Imaging and ablation were performed with Olympus FM1000-MPE system with 25x water immersion lens (XLPL25XWMP). An 800 nm laser beam was focused onto individual cranial sensory ganglion for 5 seconds when clear lesions were detected. Absence of the ablated neurons was confirmed before behavioural or calcium imaging experiments. .

Statistics

Averages of all data are shown with error bars indicating the standard error of the mean (S.E.M.). Two-tailed one sample *t*-test or Wilcoxon signed ranked test (when the data did not satisfy the assumptions of the *t*-test) were used to test if the differences between the control and treated groups. Two-tailed Student's *t*-tests or Mann-Whitney *U*-tests (when the data did not comply with the assumptions of the *t*-test) were used for two-group comparisons. ANOVAs, were used for multiple group comparisons, followed by Dunnett's or Sidak's multiple comparison test. A Linear model was built using individual data points from calcium imaging datasets. MATLAB scripts were used to perform random subsampling (function: randsample) and obtain *p* values from the linear regression analysis (function: fitlm). Prism 8 (Graphpad Software) was used for other analysis and generating plots. * indicates $p < 0.05$, ** indicates $p < 0.01$, while *** indicates $p < 0.001$.

References

1 Gautier, H. & Bonora, M. Effects of carotid body denervation on respiratory pattern of awake cats. *J Appl Physiol Respir Environ Exerc Physiol* **46**, 1127-1131, doi:10.1152/jappl.1979.46.6.1127 (1979).

2 Douglas, N. J. *et al.* Hypoxic ventilatory response decreases during sleep in normal men. *Am Rev Respir Dis* **125**, 286-289, doi:10.1164/arrd.1982.125.3.286 (1982).

3 Erickstad, M., Hale, L. A., Chalasani, S. H. & Groisman, A. A microfluidic system for studying the behavior of zebrafish larvae under acute hypoxia. *Lab Chip* **15**, 857-866, doi:10.1039/c4lc00717d (2015).

4 Kumar, P. & Prabhakar, N. R. Peripheral chemoreceptors: function and plasticity of the carotid body. *Compr Physiol* **2**, 141-219, doi:10.1002/cphy.c100069 (2012).

5 Kahlin, J. *et al.* The human carotid body releases acetylcholine, ATP and cytokines during hypoxia. *Exp Physiol* **99**, 1089-1098, doi:10.1113/expphysiol.2014.078873 (2014).

6 Soto, C. R., Ortiz, F. C., Vargas, R. V., Arroyo, J. & Alcayaga, J. Responses induced by acetylcholine and ATP in the rabbit petrosal ganglion. *Respir Physiol Neurobiol* **172**, 114-121, doi:10.1016/j.resp.2010.05.003 (2010).

7 Monteiro, E. C. & Ribeiro, J. A. Ventilatory effects of adenosine mediated by carotid body chemoreceptors in the rat. *Naunyn Schmiedebergs Arch Pharmacol* **335**, 143-148 (1987).

8 Buchanan, G. F. & Richerson, G. B. Central serotonin neurons are required for arousal to CO2. *Proc Natl Acad Sci U S A* **107**, 16354-16359, doi:10.1073/pnas.1004587107 (2010).

9 Darnall, R. A., Schneider, R. W., Tobia, C. M. & Commons, K. G. Eliminating medullary 5-HT neurons delays arousal and decreases the respiratory response to repeated episodes of hypoxia in neonatal rat pups. *J Appl Physiol (1985)* **120**, 514-525, doi:10.1152/japplphysiol.00560.2014 (2016).

10 Sundin, L., Reid, S. G., Rantin, F. T. & Milsom, W. K. Branchial receptors and cardiorespiratory reflexes in a neotropical fish, the tambaqui (Colossoma macropomum). *J Exp Biol* **203**, 1225-1239 (2000).

11 Jonz, M. G. & Nurse, C. A. Development of oxygen sensing in the gills of zebrafish. *J Exp Biol* **208**, 1537-1549, doi:208/8/1537 [pii] 10.1242/jeb.01564 (2005).

12 Jonz, M. G., Fearon, I. M. & Nurse, C. A. Neuroepithelial oxygen chemoreceptors of the zebrafish gill. *J Physiol* **560**, 737-752, doi:10.1113/jphysiol.2004.069294 jphysiol.2004.069294 [pii] (2004).

13 Perez-Garcia, M. T., Colinas, O., Miguel-Velado, E., Moreno-Dominguez, A. & Lopez-Lopez, J. R. Characterization of the Kv channels of mouse carotid body chemoreceptor cells and their role in oxygen sensing. *J Physiol* **557**, 457-471, doi:10.1113/jphysiol.2004.062281 (2004).

14 Kucenas, S., Soto, F., Cox, J. A. & Voigt, M. M. Selective labeling of central and peripheral sensory neurons in the developing zebrafish using P2X(3) receptor subunit transgenes. *Neuroscience* **138**, 641-652, doi:10.1016/j.neuroscience.2005.11.058 (2006).

15 Vladimirov, N. *et al.* Light-sheet functional imaging in fictively behaving zebrafish. *Nat Methods* **11**, 883-884, doi:10.1038/nmeth.3040 (2014).

16 Dunn, T. W. *et al.* Brain-wide mapping of neural activity controlling zebrafish exploratory locomotion. *eLife* **5**, e12741, doi:10.7554/eLife.12741 (2016).

17 Pnevmatikakis, E. A. *et al.* Simultaneous Denoising, Deconvolution, and Demixing of Calcium Imaging Data. *Neuron* **89**, 285-299, doi:10.1016/j.neuron.2015.11.037 (2016).

18 Smith, J. C., Ellenberger, H. H., Ballanyi, K., Richter, D. W. & Feldman, J. L. Pre-Botzinger complex: a brainstem region that may generate respiratory rhythm in mammals. *Science* **254**, 726-729 (1991).

19 Muniak, M. A., Ray, S., Hsiao, S. S., Dammann, J. F. & Bensmaia, S. J. The neural coding of stimulus intensity: linking the population response of mechanoreceptive afferents with psychophysical behavior. *J Neurosci* **27**, 11687-11699, doi:10.1523/JNEUROSCI.1486-07.2007 (2007).

20 Uchida, N., Poo, C. & Haddad, R. Coding and transformations in the olfactory system. *Annu Rev Neurosci* **37**, 363-385, doi:10.1146/annurev-neuro-071013-013941 (2014).

21 Sugihara, G. & May, R. M. Nonlinear forecasting as a way of distinguishing chaos from measurement error in time series. *Nature* **344**, 734-741, doi:10.1038/344734a0 (1990).

22 Takens, F. in *Dynamical Systems and Turbulence, Lecture Notes in Mathematics* Vol. 898 (ed D. A. Rand and L.-S. Young) 366–381 (Springer-Verlag, 1981).
23 Green, M. H., Curet, O. M., Patankar, N. A. & Hale, M. E. Fluid dynamics of the larval zebrafish pectoral fin and the role of fin bending in fluid transport. *Bioinspir Biomim* **8**, 016002, doi:10.1088/1748-3182/8/1/016002 (2013).
24 Alcayaga, J. *et al.* Adenosine triphosphate-induced peripheral nerve discharges generated from the cat petrosal ganglion in vitro. *Neurosci Lett* **282**, 185-188 (2000).
25 Coe, A. J., Picard, A. J. & Jonz, M. G. Purinergic and adenosine receptors contribute to hypoxic hyperventilation in zebrafish (Danio rerio). *Comp Biochem Physiol A Mol Integr Physiol* **214**, 50-57, doi:10.1016/j.cbpa.2017.09.013 (2017).
26 Shakarchi, K., Zachar, P. C. & Jonz, M. G. Serotonergic and cholinergic elements of the hypoxic ventilatory response in developing zebrafish. *J Exp Biol* **216**, 869-880, doi:10.1242/jeb.079657 (2013).
27 Surprenant, A. & North, R. A. Signaling at purinergic P2X receptors. *Annu Rev Physiol* **71**, 333-359, doi:10.1146/annurev.physiol.70.113006.100630 (2009).
28 Burnstock, G. & Wood, J. N. Purinergic receptors: their role in nociception and primary afferent neurotransmission. *Curr Opin Neurobiol* **6**, 526-532 (1996).
29 Abraira, V. E. & Ginty, D. D. The sensory neurons of touch. *Neuron* **79**, 618-639, doi:10.1016/j.neuron.2013.07.051 (2013).
30 Eatock, R. A. & Songer, J. E. Vestibular hair cells and afferents: two channels for head motion signals. *Annu Rev Neurosci* **34**, 501-534, doi:10.1146/annurev-neuro-061010-113710 (2011).
31 Icha, J. *et al.* Using Light Sheet Fluorescence Microscopy to Image Zebrafish Eye Development. *J Vis Exp*, e53966, doi:10.3791/53966 (2016).

Acknowledgements

We thank D. Thai and a number of UCSD undergraduates who helped with zebrafish care and maintenance. We also thank L.A. Hale and M. Erickstad for inputs into our behavioural setup, Uri Manor and the Waitt Advanced Biophotonics Center for imaging resources, C. Fernandes for illustrations, J. Fetcho, G. Haddad, S. Ryu, S. Navlakha, E. Mukamel, J. Wang, D. O'Keefe, C. Lee-Kubli, M. Matty, M. Rieger, A. Singh and J. How for comments on the manuscript. We are grateful to all the members of the Chalasani laboratory for critical help, advice and insights. C-M. Yeh was supported by a Salk Pioneer Fellowship. This work was funded by innovation grants from the Kavli Institute of Brain and Mind, UCSD (C-M.Y and G.M.P), Keck Foundation, National Institute of Advanced Industrial Science and Technology, Japan, (G.M.P) and Innovation grant from the Salk Institute for Biological Studies (S.H.C.).

Author contributions

C-M.Y. conceived, designed, performed experiments and co-wrote the manuscript. G.P. built theoretical models, analysed the data and co-wrote the manuscript. R.V-R., K.R. and E.D

performed experiments, A.G. designed the microfluidic device and S.H.C. conceived the experiments and co-wrote the manuscript.

Competing interests

The authors declare no competing interests.

Materials and correspondence

Requests for all materials and correspondence should be addressed to S.H.C. (schalasani@salk.edu)

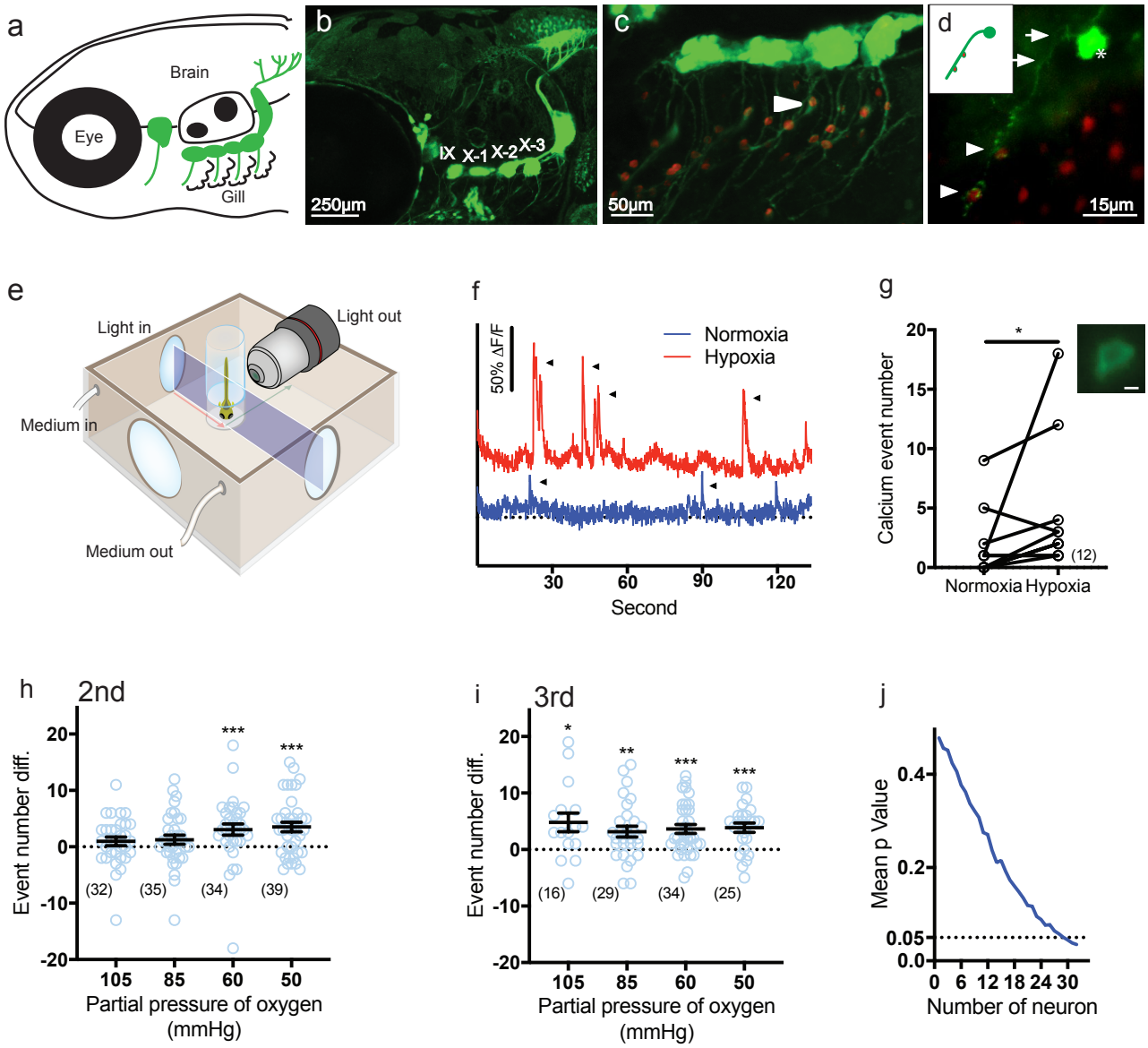

Figure 1 | Zebrafish larvae vagal sensory ganglionic neurons alter their activity upon hypoxia stimuli. a, Schematic showing the lateral view of a zebrafish larva with cranial sensory neurons and their projections labelled in green. **b,** Lateral view of a Tg(p2rx3.2:gfp) transgenic larva with the IX and X cranial sensory ganglia expressing GFP. **c,** Immunohistochemistry showing a Tg(p2rx3.2:gfp) transgenic larva with cranial sensory neurons (green) and neuroendocrine cells (red) labelled using anti-gfp (green) and anti-serotonin (red) antibodies respectively. Arrowhead indicates an example of cranial nerve afferents wrapping around neuroendocrine cells. **d,** Immunohistochemistry showing the afferent nerves of a vagal sensory neuron (green) wrapping around neuroendocrine cells (red) in a PB4;UAS:Kaede transgenic larva using anti-Kaede (green) and anti-serotonin (red) antibodies. Asterisk, arrowheads, and arrows indicate the neuron, contact sites between NECs and vagal afferents and, the neuronal projection respectively. Inset is the schematic of the neuron. **e,** Schematic showing the light-sheet microscope adapted to detect neuronal activity while the animal experiences different stimuli. **f,** Calcium data. Ratio of change in fluorescence to baseline for one representative process under normoxia and 50 mmHg hypoxia. Arrowheads indicate the calcium event detected by the software. **g,** Number of calcium events detected in the cranial sensory processes under normoxia and 50 mmHg hypoxia (n =12) with inset showing one example cranial sensory process (scale bar: 5µm). **h, i,** The difference between the number of calcium events in hypoxia and normoxia (normoxia subtracted from hypoxia) for neurons in the **(h)** 2nd (n ≥ 32) and **(i)** 3rd vagal ganglion (n ≥ 16). **j,** A linear model built on randomly subsampled data from **(h)** was used to estimate the minimal number of neurons in the 2nd vagal ganglion required to encode ambient oxygen. Averages and s.e.m. are shown in **h** and **i** with marked * indicates $p < 0.05$, while ** is $p < 0.01$ and *** shows $p < 0.001$ using Wilcoxon Matched pairs signed rank test **(j)** and One sample t-test or Wilcoxon Signed Rank test (**h** and **i**).

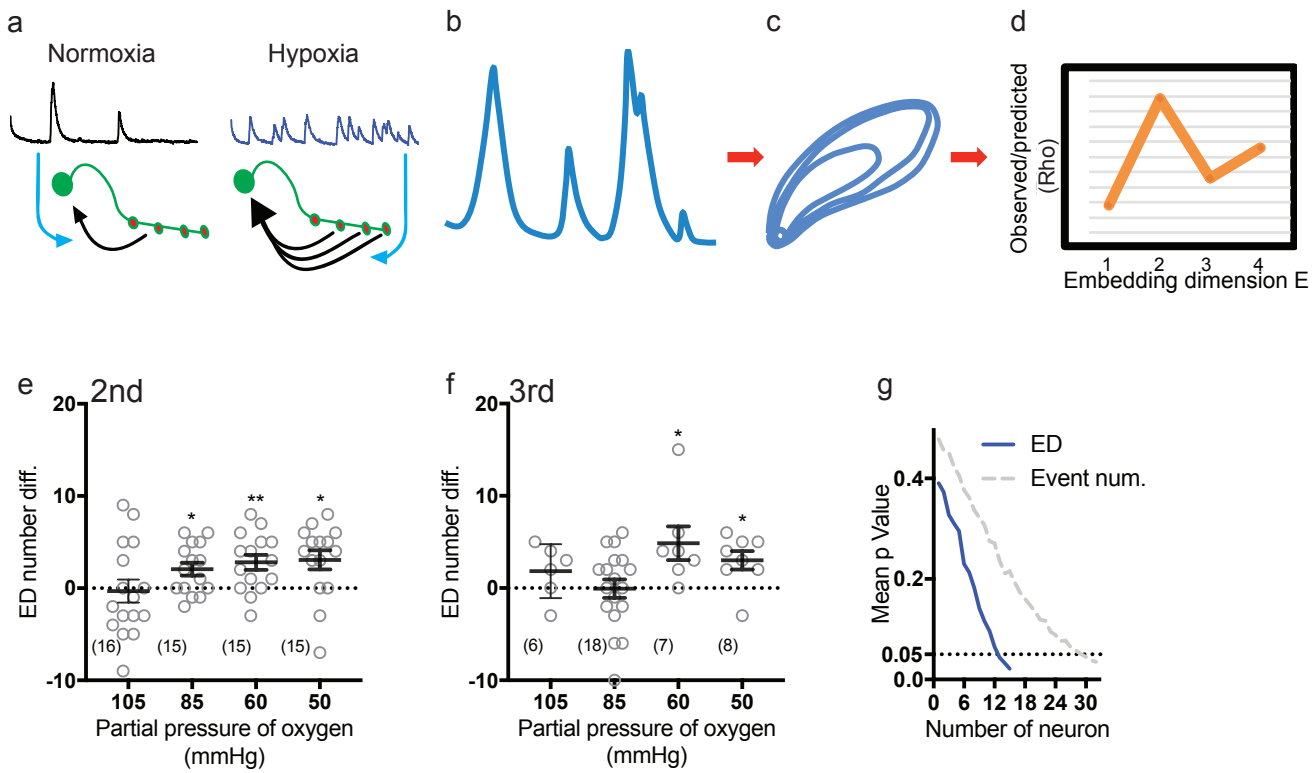

Figure 2 | Vagal sensory neurons increase their signal complexity upon hypoxia stimuli through a 'many NECs-to-one neuron' circuit. a, Schematic illustrating that the input number to individual neurons are inferred by the embedding dimension derived from the neuronal calcium traces. **b,c,d,** Outline of the dimensionality calculation using lagged coordinate embedding. **b**, We embed individual time series of GCaMP6f fluorescent signal using lags of itself into manifolds **(c)** of varying dimensionality. **d**, The dimensionality that best predicts the withheld out of sample data (i.e. with highest observed/predicted rho) is probably closest to the correct dimension of the observed neuron within the bounds given by the Whitney embedding theorem. **e, f,** Embedding dimension difference between hypoxia and normoxia (normoxia subtracted from hypoxia) for neurons in the **(e)** 2nd ($n \geq 15$) and **(f)** 3rd ($n \geq 6$) vagal ganglion. **g,** A linear model built on randomly subsampled embedding dimensions from neurons in the 2nd vagal ganglion was used to estimate the number of neuron required to encode ambient oxygen. For comparison, dashed line showed the result from the same method with calcium event number as input (Fig. 1j). Averages and s.e.m. are shown in **e** and **f** with marked * indicates $p < 0.05$, while ** is $p < 0.01$ using One sample t-test or Wilcoxon Signed Rank test (**e** and **f**).

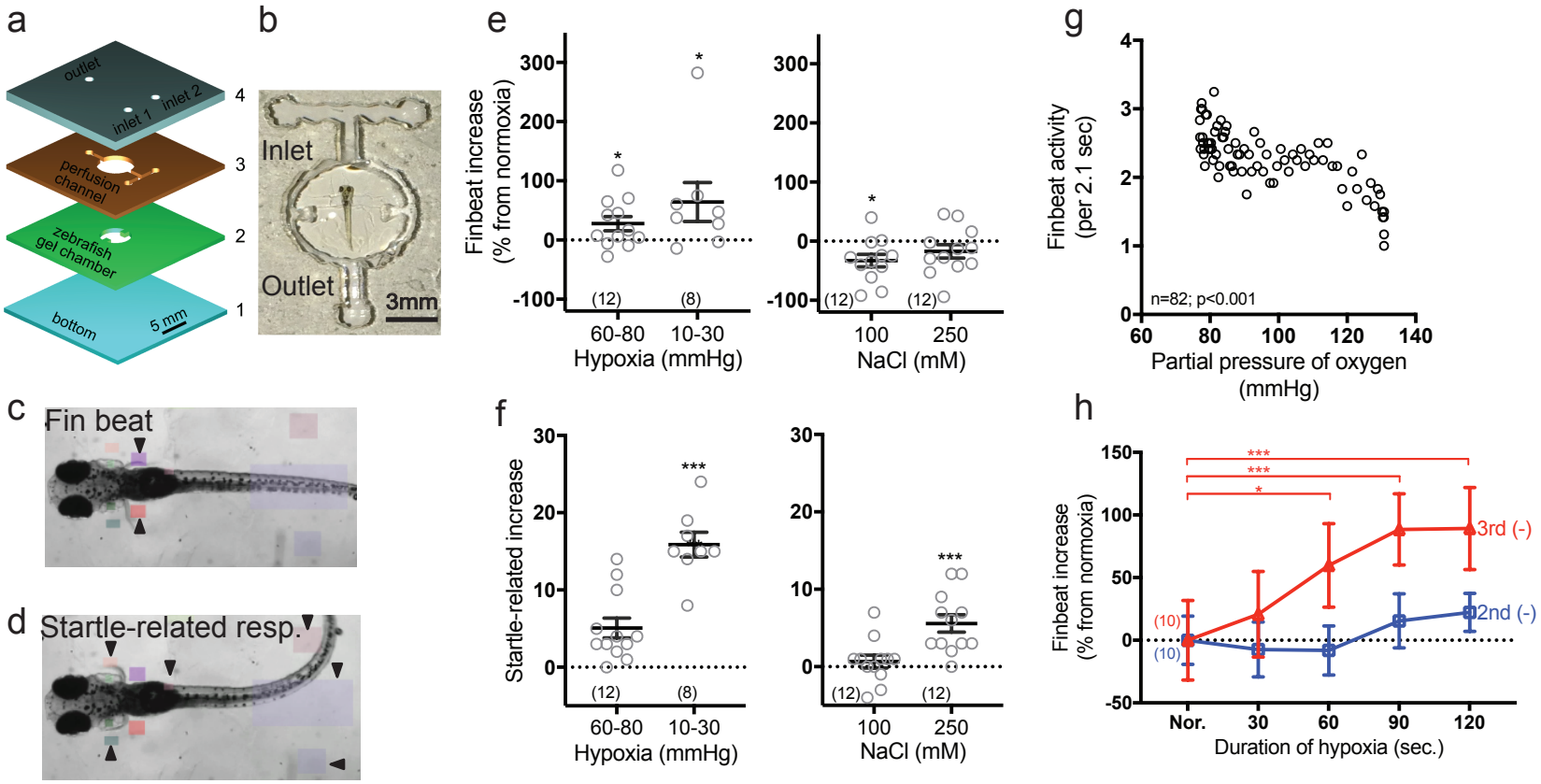

Figure 3 | 2nd vagal sensory neurons drive hypoxia-induced respiratory behaviour. a, Schematic showing the acrylic-based microfluidics device that can trap **(b)** larva and monitor behaviours while delivering oxygen stimuli. Regions of interest (lightly shaded boxes identified by black arrowheads) for identifying **(c)** fin beats and **(d)** startle-related responses in larva. **e, f,** Animals were exposed to hypoxia or osmotic shock and the increases in number of fin beats **(e)** ($n \geq 8$) and startle-related responses **(f)** ($n \geq 8$) from controls are shown. **g,** Rate of pectoral fin beats is inversely proportional to ambient oxygen levels ($n = 82$). **h,** Average number of pectoral fin beats in animals without 2nd and 3rd vagal sensory ganglionic neurons experiencing hypoxia ($n \geq 10$). Averages and s.e.m. are shown in **e, g, h** with * indicates $p < 0.05$, while ** is $p < 0.01$ and *** shows $p < 0.001$ using one sample t-test **(e, g)** and two-way ANOVA with Dunnett's multiple comparison **(h)**.

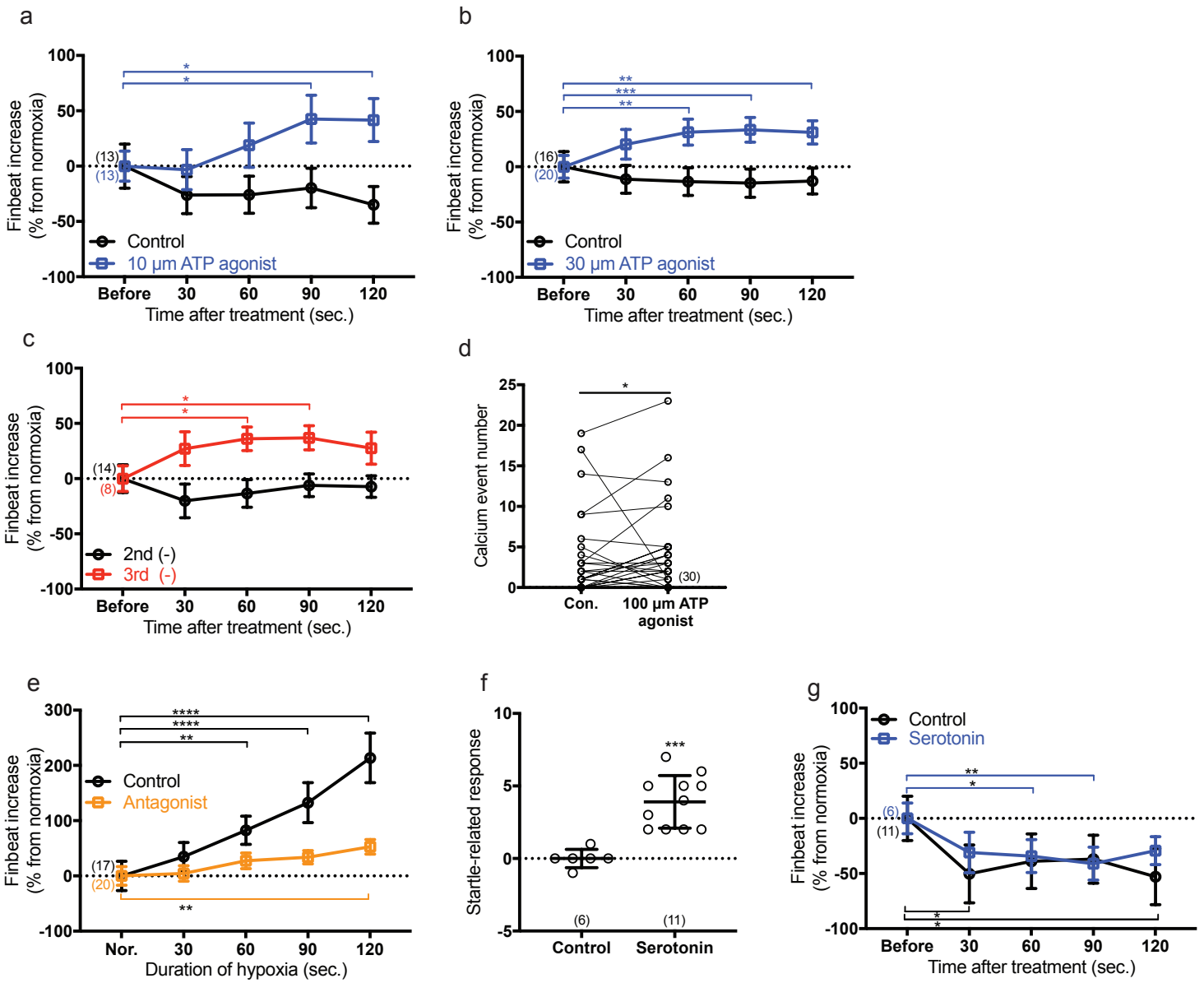

Figure 4 | Purinergic signalling enhances activity of neurons in 2nd vagal sensory ganglion and initiate hypoxia-induced pectoral fin beats. a,b, Average number of fin beats in animals exposed to **(a)** 10 µm and **(b)** 30 µm P2 purinoceptor agonist (α,β-methyleneadenosine 5'-triphosphate trisodium salt) (n ≥ 13). **c,** Average fin beats in agonist-treated animals missing neurons in the 2nd or 3rd vagal sensory ganglia (n ≥ 8). **d,** 2nd vagal ganglionic neuronal calcium events in animals experiencing 100 µm of P2 purinoceptor agonist (n = 30). **e,** Average fin beat rate in animals treated with 100 µm of PPADS, a P2 purinoceptor antagonist (n ≥ 17). **f, g,** The changes in startle-related responses **(f)** and average number of pectoral fin beats **(g)** (n ≥ 6) in larvae exposed to 4 mM serotonin. Averages and s.e.m. are shown with * indicates $p < 0.05$, while ** is $p < 0.01$ and *** shows $p < 0.001$ obtained using two-way ANOVA with Sidak's multiple comparisons (**a-c, e** and **g**), Wilcoxon Matched pairs signed rank test **(d)** and One sample t-test **(f)**.